Available online at www.sciencedirect.com
ScienceDirect
Journal of Hazardous Materials 152 (2008) 616–623
Journal of Hazardous Materials
www.elsevier.com/locate/jhazmat

Mercury emissions from coal combustion: Modeling and comparison of Hg capture in a fabric filter versus an electrostatic precipitator

Fabrizio Scala [a,*], Herek L. Clack [b,1]

[a] *Istituto di Ricerche sulla Combustione, Consiglio Nazionale delle Ricerche, P. le Tecchio, 80-80125 Napoli, Italy*
[b] *Department of Mechanical, Materials, and Aerospace Engineering, Illinois Institute of Technology, Chicago, IL 60616, USA*

Received 7 August 2006; received in revised form 9 July 2007; accepted 10 July 2007
Available online 17 July 2007

Abstract

Mercury emissions from coal combustion must be reduced, in response to new air quality regulations in the U.S. Although the most mature control technology is adsorption across a dust cake of powdered sorbent in a fabric filter (FF), most particulate control in the U.S. associated with coal combustion takes the form of electrostatic precipitation (ESP). Using recently developed models of mercury adsorption within an ESP and within a growing sorbent bed in a FF, parallel analyses of elemental mercury (Hg^0) uptake have been conducted. The results show little difference between an ESP and a FF in absolute mercury removal for a low-capacity sorbent, with a high-capacity sorbent achieving better performance in the FF. Comparisons of fractional mercury uptake per-unit-pressure-drop provide a means for incorporating and comparing the impact of the much greater pressure drop of a FF as compared to an ESP. On a per-unit-pressure-drop basis, mercury uptake within an ESP exhibited better performance, particularly for the low-capacity sorbent and high mass loadings of both sorbents.

Keywords: Mercury capture; Coal combustion; Fabric filter; Electrostatic precipitator; Adsorption model

1. Introduction

Coal-fired power plants (CFPPs) are the most difficult mercury emissions source facing control under the 2005 Clean Air Mercury Rule (CAMR) issued by the U.S. EPA. Unlike municipal and medical waste incinerators (MWIs) which emit much higher concentrations of mercury that is almost exclusively in the oxidized form Hg^{2+}, CFPPs emit very dilute (single ppb) concentrations of both elemental (Hg^0) and oxidized (Hg^{2+}) mercury, whose proportions in relation to the total mercury load can vary widely. Because Hg^{2+} is more condensable and far more water-soluble than Hg^0, the large variability in mercury speciation in CFPP exhaust translates into large uncertainty in the total mercury removal efficiency of most mercury emissions control technologies.

Pilot and full-scale studies have shown that fixed sorbent beds, a control approach adopted from MWIs, can achieve 90% or greater removal efficiency for both mercury species at carbon-to-mercury ratios of 10,000:1 to 15,000:1 [1]. Whereas fabric filters (FFs) are common among MWIs, they are installed on only about 10% of coal-fired boilers in the U.S. [2]. About three-quarters of coal-fired boilers in the U.S. employ electrostatic precipitators (ESPs) for particulate control [2]. The comparable pilot- and full-scale data for mercury capture within ESPs generally exhibit significantly greater scatter, but ESPs are typically understood to require greater amounts of carbon to achieve the same removal efficiency as FFs at comparable temperatures (particularly at low carbon-to-mercury (C:Hg) ratios), with maximum observed removal efficiencies of about 65–70% [1,3]. Despite the pilot- and full-scale data, until recently [4–6], the mass transfer mechanisms for mercury capture within an ESP were only incompletely understood, thereby preventing modeling, optimization, or comparison between ESPs and FFs in any degree of detail. Such modeling is important because it enables more thorough comparisons between fabric filters (which exhibit higher Hg capture efficiencies at a given C:Hg ratio) and ESPs

* Corresponding author. Tel.: +39 081 768 2969; fax: +39 081 593 6936.
E-mail addresses: scala@irc.cnr.it (F. Scala), herek.clack@iit.edu (H.L. Clack).
[1] Tel.: +1 312 567 3184; fax: +1 312 567 7230.

0304-3894/$ – see front matter © 2007 Elsevier B.V. All rights reserved.
doi:10.1016/j.jhazmat.2007.07.024

(which are widely used in the U.S.). Further, although the per-unit-sorbent-mass costs of Hg adsorption in a fixed bed are understood to be lower than those of ESPs, no comparison has been made on a per-unit-pressure-drop basis. This metric is relevant because the large number of CFPPs operating with ESPs essentially have two adsorption-based retrofitting options for mercury capture: installation of a sorbent injection system upstream of the existing ESP, or installation of both a sorbent injection system and baghouse downstream of the existing ESP. The pressure drop of a retrofitted FF is likely to be roughly an order of magnitude greater than that of the existing ESP. Thus, just as higher per-unit-sorbent-mass costs increase the operating expense of Hg capture within an ESP, so too may higher per-unit-pressure-drop costs increase the overall expense of Hg capture in a retrofitted FF. These costs are associated with powering induced draft (ID) fans that may be required to overcome the additional pressure drop, as well as the capital costs to reinforce ductwork to resist collapse under the increased vacuum (gauge pressure) upstream of the FF.

Practical and facility constraints largely preclude taking parallel, simultaneous pilot- or full-scale mercury capture data for a FF and an ESP for direct comparison. Further, because flue gas composition is highly variable, analyses that minimize this variability will yield broadly applicable results which address those phenomena other than chemical kinetics that affect mercury adsorption. An analytical or numerical comparison of mercury capture within FFs and ESPs is only recently possible with the development of gas-particle mass transfer models applicable to electrostatic precipitation [4–6], in addition to those applicable to fabric filters [7–10]. Such model results would not only enable comparisons of both absolute and per-unit-sorbent mercury capture, but also mercury capture on a per-unit-pressure-drop basis by incorporating semi-empirical pressure drop correlations for fabric filters as the collected particle loading increases (compared to a FF, the pressure drop across an ESP is constant). The present analysis provides the first direct comparison of mercury capture within a FF and an ESP, considering both a high-capacity and a low-capacity sorbent, thereby establishing the broader implications to be considered in devising a cost-effective mercury emissions control approach.

2. Theory

The proposed model is based on the following simplifying assumptions:

1. Mercury exists only as Hg^0 in the gas phase (this provides a conservative measure of total ($Hg^0 + Hg^{2+}$) mercury removal.
2. Mercury adsorption is independent of flue gas composition.
3. Sorbent particles are spherical, of uniform diameter, and are uniformly dispersed in the dust cake of the FF and in the cross-stream direction in the ESP (but vary with stream-wise position).
4. Both the gas and solid flow rates are constant.
5. The temperature is constant and uniform through the system.
6. Mercury adsorption at the surface of the activated carbon particle is based on local equilibrium conditions between the gas and the adsorbed phases, according to the Langmuir theory. Radial gradients of mercury concentration inside the particle are neglected. This assumption implies that model results will represent the upper limit for the mercury removal efficiency.
7. Negligible adsorption occurs upstream of the particulate control device (ESP or fabric filter) [8–11].

The process of mercury vapor adsorption onto activated carbon is schematized as a series of two steps: mass transfer from the bulk gas to the external surface of the activated carbon particle through the gas boundary layer and surface adsorption in the particle.

The first step is treated by means of an external mass transfer coefficient determined by the particle Sherwood number. Regarding the second step, considerable uncertainty exists on the mechanism of elemental mercury adsorption on virgin or impregnated activated carbon particles. There is evidence that a physical adsorption mechanism should be relevant for virgin activated carbons, while both chemisorption and physical adsorption have been suggested for impregnated carbons [10]. Many theoretical and empirical equations can be used to model both physical and chemical adsorption processes. In the present analysis, the Langmuir theory will be used. Langmuir isotherms were successfully used to correlate experimental adsorption data [12,13], with the caveat that such data were obtained in a nitrogen gas stream. Conversely, it has been reported that the flue gas composition exerts a considerable influence on the mercury uptake [10]. Due to the lack of thermodynamic adsorption data obtained under simulated flue gas conditions, however, data obtained under nitrogen stream have been considered for the present analysis.

Although sorbent injection for mercury capture within a FF or an ESP may involve mixed flows of powdered sorbent and fly ash, no contribution of the fly ash to mercury capture is considered here.

2.1. Model equations

Following the Langmuir theory, the equilibrium gas phase mercury concentration (c^*) can be related to the adsorbed mercury uptake on the activated carbon particle (ω^*, kg Hg/kg sorbent) by:

$$c^* = \frac{1}{K_{eq}} \left(\frac{\omega^*/\omega_{max}}{1 - \omega^*/\omega_{max}} \right) \quad (1)$$

where K_{eq} is the adsorption equilibrium constant, and ω_{max} is the maximum mercury uptake capacity.

The analyses of the fabric filter and ESP mercury capture processes are detailed separately in the following sections.

2.1.1. Fabric filter mercury capture

The system is schematized as an activated carbon fixed bed (dust cake) of growing thickness. The effects of pressure drop change and flow redistribution on mercury removal in the fabric filter have been assumed to be negligible [14]. The flue gas is assumed to travel in plug flow along the filter cake, and

axial dispersion is neglected [8]. Typical superficial gas velocities through fabric filters (air-to-cloth ratio) are of the order of 0.005–0.05 m/s. In light of the very low gas/sorbent relative velocities a reasonable assumption is that the particle Sherwood number is equal to the limiting theoretical value of $2\varepsilon_{bed}$ relative to the stagnant boundary layer condition, where the bed (cake) porosity ε_{bed} accounts for the reduced volume available for diffusion.

The mercury mass balances in the bulk gas phase and in the adsorbed phase in a filter cake section are as follows:

$$\varepsilon_{bed}\frac{\partial c}{\partial t} + v\frac{\partial c}{\partial z} = -\frac{3\rho_{bed}}{\rho_P R_P}K_G(c - c^*) \quad (2)$$

$$\frac{\partial \omega}{\partial t} = \frac{3}{\rho_P R_P}K_G(c - c^*) \quad (3)$$

where c is the bulk gas mercury concentration, ω the adsorbed mercury uptake on the activated carbon particle, v the superficial gas velocity in the cake, ρ_P the sorbent particle density, $\rho_{bed} = \rho_P(1 - \varepsilon_{bed})$ is the cake density, and R_P is the sorbent particle radius. The boundary layer mass transfer coefficient is given by $K_G = D_m Sh/2R_P$ (D_m is the molecular mercury diffusion coefficient).

The system of two coupled differential equations (Eqs. (2) and (3)) has the following initial and boundary conditions:

$$\omega(z, 0) = 0; \quad c(z, 0) = 0 \quad (4)$$

$$c(0, t) = c^{IN} \quad (5)$$

where c^{IN} is the inlet mercury bulk concentration. The actual cake thickness can be calculated as:

$$L(t) = v_d t \quad (6)$$

The sorbent deposition velocity on the filter is given by:

$$v_d = \frac{\Theta_{AC} v}{\rho_{bed}} \quad (7)$$

where Θ_{AC} is the activated carbon loading per-unit-volume in the bulk gas.

To solve the system of Eqs. (1)–(3) (with initial and boundary conditions, Eqs. (4) and (5)), they have been non-dimensionalized by means of suitable variables [8]. It is interesting to note that as the final cake thickness ($L_F = v_d t_F$, where t_F is the total filtration time) is proportional to the superficial gas velocity in the cake (see Eqs. (6) and (7)), the system of Eqs. (1)–(3) is independent of v.

The boundary-value partial differential problem was solved using an orthogonal collocation technique [15]. To account for the moving boundary nature of the problem (growing thickness of the cake), a suitable change of variables to immobilize the moving front was performed adopting a set of transformation rules of the partial derivatives to account for the displacement of the collocation points in the domain with time [10]. After the above manipulations, fictitious partial derivatives along the dimensionless cake thickness are introduced in Eqs. (2) and (3). Immobilization of the moving front with this technique enables the boundary-value partial differential problem along the cake thickness to be reduced to a set of $2n$ initial-value ordinary differential equations in time using orthogonal collocation. To this end, the solution was approximated by a linear combination of Lagrange polynomials and the collocation points were chosen as the zeroes of Legendre polynomial of the same order as the number of internal collocation points. The resulting system of ordinary differential equations was integrated using a 5th order Runge-Kutta method with adaptive stepsize control. The number of collocation points (n) and the Runge-Kutta stepsize were adjusted in order to give a total accuracy of 10^{-4} in the value of the output variables. Accordingly a value of $n = 5$ was used for the calculations.

2.1.2. ESP mercury capture

Mercury capture within an ESP consists of in-flight adsorption by the suspended powdered sorbent particles, which predominates, and a smaller contribution from the PM collected on the plate electrodes. For brevity, the present analysis focuses on the in-flight adsorption mechanism. Surface adsorption of mercury by the dust cake on the ESP plate electrodes is small [4] and thus neglected as a second order effect.

Consider a generic turbulent channel flow between two plate electrodes of length L and separated by spacing H within an ESP, half of which is shown in Fig. 1. The present analysis assumes values of $H = 0.5$ m and $L = 12$ m, although ESP specifications vary widely in practice. The pressure is 101.325 kPa and the flow velocity ($U = 3$ m/s) is uniform entering the channel.

The charged sorbent particles suspended within the gas entering the ESP have a uniform diameter d_p. Most often, turbulent conditions exist within an ESP [16,17], reflecting either a super-

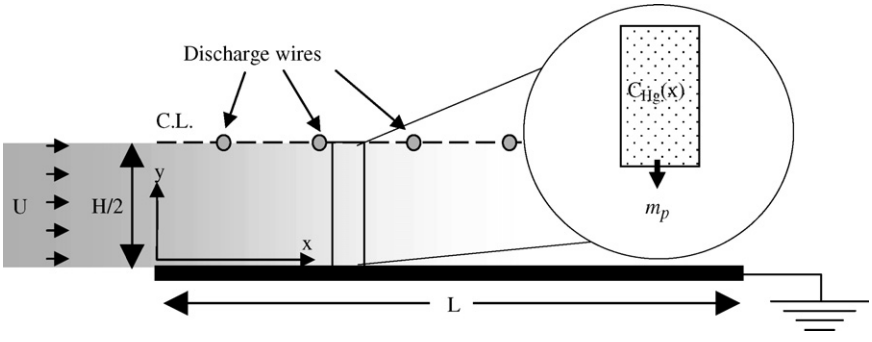

Fig. 1. Schematic of one-half of a channel between two plate electrodes of an ESP for turbulent conditions (drawing not to scale).

critical channel Reynolds number or electro-hydrodynamic effects (i.e., "corona wind"). The Deutsch-Anderson equation [17,18] relates the stream-wise (x-direction, Fig. 1) decay in particle number density in the channel as charged particles drift toward and are collected on the plate electrodes that form the channel walls. A fundamental assumption underlying the Deutsch-Anderson equation is that turbulence in the channel is sufficiently vigorous and turbulent diffusivity sufficiency large that uniform scalar quantities are maintained in the transverse flow direction (y-direction, Fig. 1). Consequently, the electrostatic precipitation of the suspended sorbent particles produces a stream-wise decay in both particle mass loading and Hg^0 concentration. It has been established that assumptions of infinite turbulent diffusivity during electrostatic precipitation represents an upper limit to ESP collection efficiency [19]. Further, the size and density of the sorbent particles are such that their transient response times are generally less than a fraction of a millisecond [6], shorter than characteristic turbulence time scales. As a result, the equilibrium between Coulombic and drag forces that dictates the relative velocity between the gas and the particle (gas-particle "slip") remains undisturbed even in the presence of turbulent fluid velocity fluctuations. Such turbulent fluctuations strongly impact the particle motion in an inertial reference frame, but the particle velocity relative to the gas remains essentially constant. It is the relative velocity between the particle and the gas on which particle Reynolds number is based; thus the convective mass transfer characteristics of the particle, as indicated by the Reynolds number-dependent Sherwood number, are constant for a specified particle size and electrostatic drift velocity.

Crowley [20] gives the terminal electrostatic drift velocity of a particle of diameter d_p as (Eq. (8)):

$$U_{es}(d_p) = \frac{neEC_c}{3\pi\mu d_p} \tag{8}$$

where e is the value of an elementary charge, i.e. an electron ($4.8e^{-10}$ stC), n the number of elementary charges retained by the particle, E the electric field strength [stV/cm], C_c the Cunningham slip correction factor for Stokes drag on small particles, and μ is the dynamic viscosity of air [dyn s/cm^2].

In an ESP, particles are charged both by field charging (Eq. (9)) [21] and diffusion charging (Eq. (10)) [16]:

$$n = \left[1 + 2\frac{\varepsilon - 1}{\varepsilon + 2}\right]\frac{Ed_p^2}{4e} \quad \text{(Field charging)} \tag{9}$$

$$n = \frac{d_p kT}{2e^2}\ln\left[1 + \left(\frac{2\pi}{m_i kT}\right)^{1/2} d_p e^2 n_{i\infty} t\right] \quad \text{(Diffusion charging)} \tag{10}$$

where n is the number of unit charges on a particle, e the charge of an electron [stC], k the Boltzmann's constant [erg/K], T the temperature [K], E_o the electric field strength in the channel [stV/cm], ε the particle dielectric constant (assumed to be very large), m_i the mass of a gaseous ion (assumed to be O_2) [g], t the time [s], and $n_{i\infty}$ is the ion density far from the particle [cm^{-3}]. Whereas the equilibrium particle charge is attained nearly instantaneously by field charging, diffusion charging occurs more slowly. Thus, the equilibrium particle charge by diffusion charging is taken as the average over the characteristic fluid time scale of the channel, L/U. The total particle charge is the sum of the equilibrium field and diffusion charges, although additive approaches to particle charging are generally less accurate than numerical modeling of the charging process [21].

Using Eqs. (8)–(10), a modified form of the Deutsch-Anderson equation (Eq. (11)) predicts an exponential decay in the sorbent particle number density ND_p with t (or, alternatively, with x in Fig. 1), assuming neither physical or electrical particle interactions:

$$ND_p(t) = ND_{p,0}\exp\left[-2U_{es}(d_p)\frac{t}{H}\right] \tag{11}$$

where $ND_{p,0}$ and $U_{es}(d_p)$ are the initial number density entering the channel and the terminal electrostatic drift velocity, respectively, of particles of diameter d_p.

The Frössling equation [22] provides a correlation between the mean Sherwood number about a spherical particle $\overline{Sh_d}$ and the particle Reynolds number which depends on the gas-particle slip velocity induced by the total particle charge and the electric field within the channel. Using the definition of $\overline{Sh_d}$, the mean convective mass transfer coefficient $\overline{h_m}$ can be determined (Eq. (12)) using the molecular diffusivity D_{ab} (see Section 2.2).

$$\overline{Sh_d} = \frac{\overline{h_m}d_p}{D_{ab}} = 2 + 0.552Re_d^{1/2}Sc^{1/3} \tag{12}$$

For a particular particle diameter d_p, a specified particle charge and electric field strength lead to a constant gas-particle slip velocity, constant particle Reynolds number Re_d, and a constant mean convective mass transfer coefficient, $\overline{h_m}$. Thus, the rate of change of Hg^0 concentration within a differential volume within the channel (Eq. (13)) is determined by the cumulative rate of Hg^0 uptake by the particles in the flow (Eq. (14)):

$$\rho\,\Delta V\frac{\partial C_V}{\partial t} = -\dot{M}_{Hg}(t) \tag{13}$$

$$\dot{M}_{Hg}(d_p, t) = \overline{h_m}(d_p)ND_p(d_p, t)\,\Delta V 4\pi\left(\frac{d_p}{2}\right)^2\rho(C_V(t) - c^*(t)) \tag{14}$$

The number density $ND_p(d_p,t)$ of particles is determined from Eq. (11) and using the initial sorbent mass loading ML_p and the particle diameter d_p and density (given in Table 1 for the two sorbents).

Table 1
Adsorptive and physical properties of the sorbents considered

Sorbent	K_{eq} (m^3/g)	ω_{max}	ρ_P (kg/m^3)
HGR	422	2.2e−2	990
DARCO G60	420	1.07e−4	750

2.2. Parameters estimation

The model was applied to one virgin activated carbon (DARCO G60) and one sulfur impregnated carbon (HGR). Adsorptive and physical properties of the sorbents considered were taken from literature [12,13] and are reported in Table 1. Molecular diffusivity of elemental mercury in the flue gas was estimated by means of the Chapman–Enskog theory and was calculated to be 0.24×10^{-4} m^2/s at 150 °C. A bed porosity value $\varepsilon_{bed} = 0.5$ was used in the fabric filter model calculations.

3. Results and discussion

The values and range of the input variables were chosen in order to simulate as closely as possible typical coal-fired power plants operating conditions. Base case calculations have been performed for the two activated carbons at a temperature of 150 °C and an inlet elemental mercury bulk concentration of 5 μg/m^3.

3.1. Fabric filter mercury capture

Figs. 2 and 3 show the filter outlet gas bulk mercury concentration as a function of filtration time, parametric in the sorbent loading and in the sorbent particle size, respectively, for the two activated carbons considered. The outlet gas bulk mercury concentration has been normalized with the inlet one. The outlet mercury concentration curves show that contrary to typical fixed bed operation, the outlet mercury concentration decreases with filtration time until an asymptotic figure is approached. This behavior is the consequence of the growing thickness of the cake: fresh sorbent is continuously added on the filter providing increased mercury adsorption. At long times, however, the ending zone of the cake gives a negligible contribution to the adsorption process so that asymptotic conditions are reached. Comparison of the curves shows that a dramatic difference exists between HGR and DARCO G60 carbons, the former performing considerably better under the same operating conditions. It is

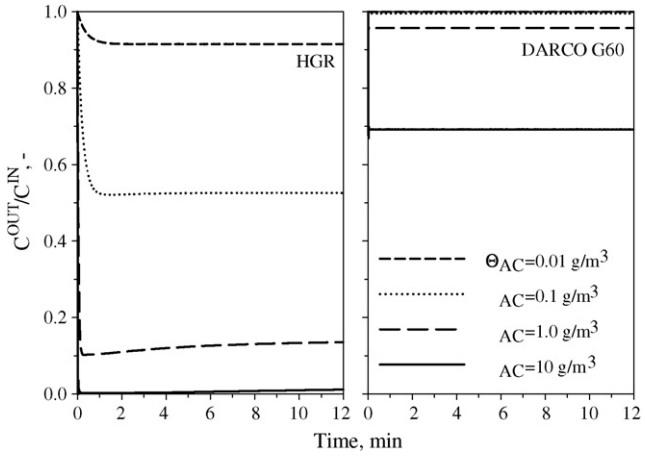

Fig. 2. Filter outlet gas bulk mercury concentration as a function of filtration time for different activated carbon loadings. Sorbent: HGR (left), DARCO G60 (right); $T = 150$ °C; $c_B^{IN} = 5$ μg/m^3; $d_p = 20$ μm.

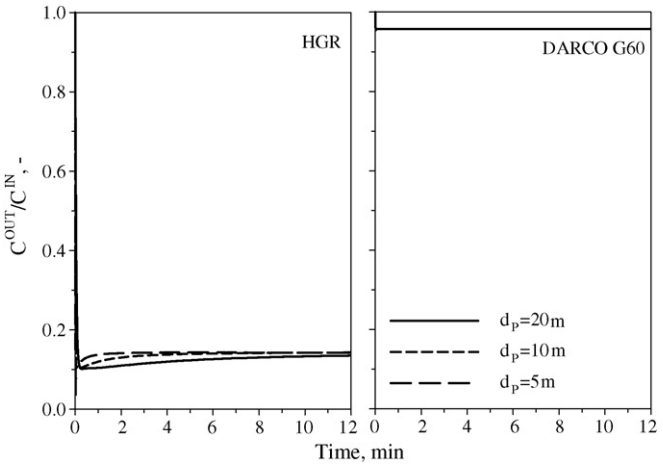

Fig. 3. Filter outlet gas bulk mercury concentration as a function of filtration time for different particle sizes. Sorbent: HGR (left), DARCO G60 (right); $c_B^{IN} = 5$ μg/m^3; $\Theta_{AC} = 1.0$ g/m^3.

interesting to note that for the virgin carbon the initial transient is practically instantaneous and steady outlet conditions are rapidly reached. This is a consequence of the very low mercury uptake capacity of this sorbent compared to the sulfur impregnated one.

The effect of the sorbent loading on mercury capture (Fig. 2) is straightforward: larger carbon loadings lead to much larger mercury captures on the filter for both carbons. On the other hand, the sorbent particle size (Fig. 3) influenced marginally the concentration profiles. Only the initial transient is slightly affected by this variable, in the sense that steady outlet conditions are attained more rapidly when smaller particles are used.

The analysis thus far has been restricted to the mercury capture behavior of a single fabric filter section. Full-scale baghouses generally consist of many compartments cleaned cyclically in a staggered way. It was noted by Scala [8] that while the mean outlet mercury concentration does not vary with the number of compartments, a large number of compartments gives a smoother mercury removal operation avoiding large concentration spikes at the baghouse outlet. In the following, the mean mercury removal (calculated from the mean outlet gas bulk mercury concentrations) will be considered in order to have curves independent of the number of compartments. To simulate a real full-scale baghouse performance a cycle time typical of a pulse-jet baghouse ($t_F = 12$ min) was chosen.

Fig. 4 reports the mean gas bulk mercury removal as a function of the sorbent loading for the two activated carbons considered. The curves show that in order to obtain mercury removal efficiencies of the order of 90–95%, loadings of the order of 1–10 g/m^3 have to be used with HGR, while larger figures are necessary with DARCO G60. It must be emphasized that these results are based on the implicit assumption of idealized baghouses. Should non-ideal phenomena, often observed during pulse-jet baghouse operation, like patchy cleaning or ash re-entrainment after pulsing be relevant, the performance might be different.

Overall, the model results indicate that mercury capture in coal-fired power plant flue gas can be performed on the fabric filter cake with high removal efficiencies and with moderate sor-

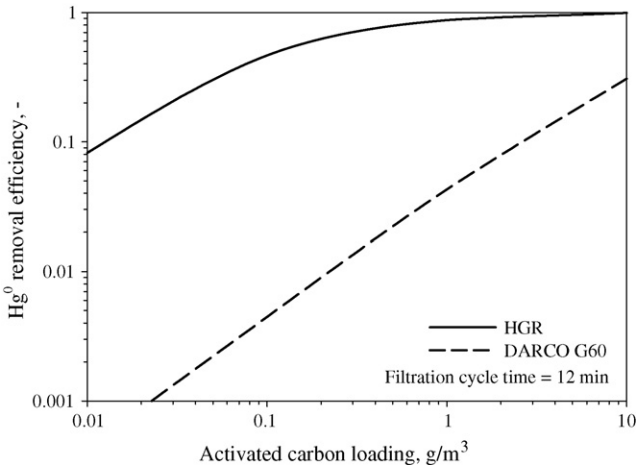

Fig. 4. Mean gas bulk mercury removal in a pulse-jet baghouse as a function of activated carbon loading, for HGR and DARCO G60 carbons. $d_p = 20\,\mu m$; $c_B^{IN} = 5\,\mu g/m^3$; $t_F = 12\,min$.

bent consumption, provided an activated carbon with sufficiently high uptake capacity is used.

3.2. ESP mercury capture

Similar to Fig. 2 for the fabric filter analysis, Fig. 5 compares the mercury capture of DARCO G60 against the higher capacity HGR sorbent as a function of particle mass loading. The trends are similar to those in Fig. 2 for the fabric filter, namely that the DARCO G60 exhibits capacity-limited adsorption behavior, with only the 1 and 10 g/m^3 sorbent mass loading values achieving appreciable Hg^0 removal. Note the different time scales used in Figs. 2 and 5; the relevant time scale for the ESP is the fluid residence time, while for the fabric filter it is the bag cleaning cycle. The capacity-limited nature of the DARCO G60 sorbent is apparent in the absence of transient uptake behavior even on the much shorter time scales of the ESP analysis (Fig. 5). The depletion of the DARCO G60 Hg^0 capacity is sufficiently rapid that the final residual Hg^0 fraction (C^{out}/C^{in}) at each sorbent mass loading value (Θ_{AC}) is the same for both ESP and fabric filter analyses.

As was the case in the fabric filter analyses, the in-flight adsorption performance of the HGR sorbent within the ESP achieved much lower residual Hg^0 fractions at all sorbent mass loading values (Fig. 6). The higher capacity of the HGR reveals the differences in gas-particle mass transfer between the in-flight adsorption occurring within the ESP and the fixed bed adsorption in the fabric filter. For particle mass loading $\Theta_{AC} = 1\,g/m^3$, the ESP results predict a residual mercury fraction of 0.5, whereas the same Θ_{AC} value in the fabric filter results produced a significantly lower residual mercury fraction, less than 0.2. Part of the difference can be traced to the decreasing sorbent mass loading through the ESP. At 2 s, 90% of the initial sorbent mass of 20 mm particles has been removed. While the rapid collection supports higher particle Reynolds and Sherwood numbers, the increased gas-particle mass transfer is not enough to compensate for the loss of sorbent mass due to collection. Because particle size distribution strongly impacts gas-particle mass transfer within an ESP [6], only limited conclusions can be generalized to actual ESPs. As was the case previously for sorbent mass loading (Fig. 5), the higher capacity HGR sorbent reveals sensitivities of gas-particle mass transfer that the lower-capacity DARCO G60 does not. In Fig. 6, the sensitivity of gas-particle mass transfer within an ESP to particle size (and, by extension, particle size distribution) is apparent for the HGR sorbent but not for the DARCO G60. This contrasts with the relative insensitivity of fixed bed adsorption to sorbent particle size for both sorbents (see fabric filter analysis, Fig. 3).

Similar to earlier comparisons between ESPs and FFs on the basis of mercury removal efficiency per-unit-sorbent-mass (e.g., Figs. 2 and 5), Fig. 7 compares ESPs and FFs on the basis of fractional mercury uptake per-unit-pressure-drop. A representative pressure drop of 62.5 Pa (1/4 in. H_2O) was used in the ESP

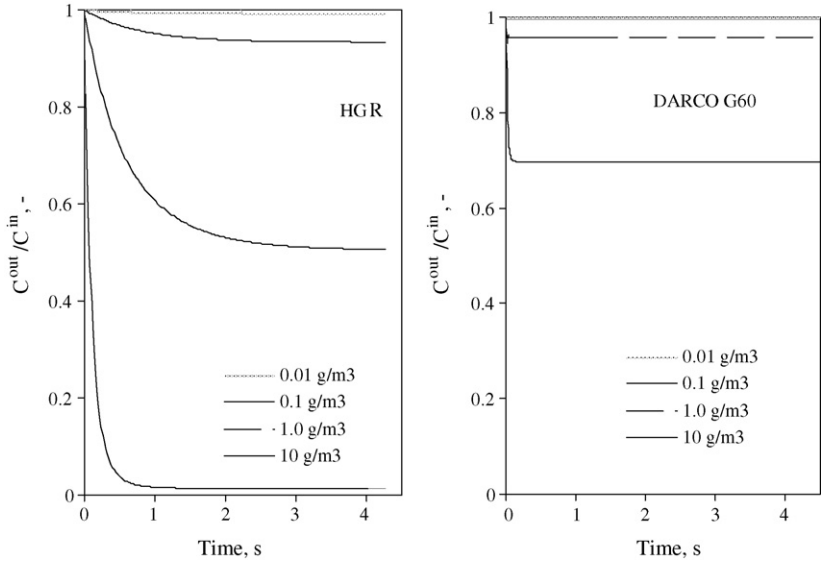

Fig. 5. Residual mercury fractions for HGR (left) and DARCO G60 (right) as a function of sorbent mass loading Θ_{AC}. $d_p = 20\,\mu m$; $c_B^{IN} = 5\,\mu g/m^3$; $E = 200\,kV/m$.

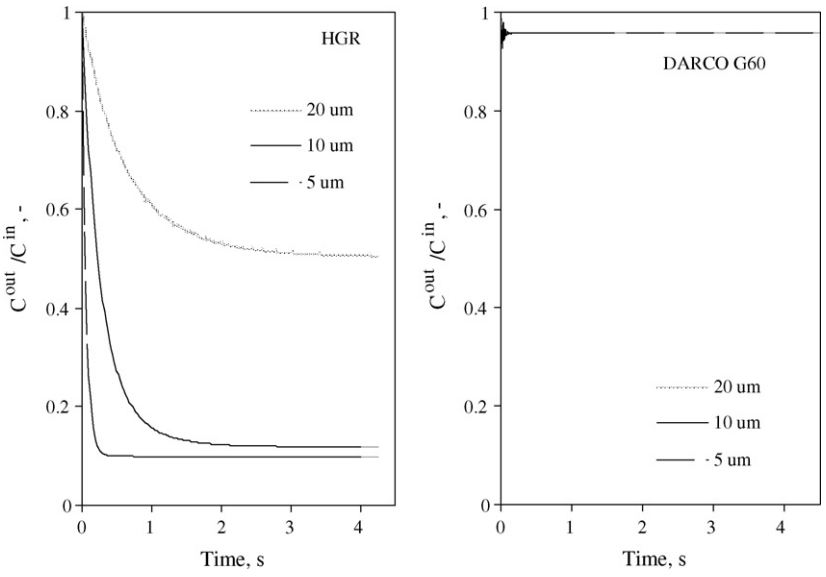

Fig. 6. Residual mercury fractions for HGR (left) and DARCO G60 (right) as a function of sorbent particle size d_p. $\Theta_{AC} = 1.0\ g/m^3$; $c_B^{IN} = 5\ \mu g/m^3$; $E = 200\ kV/m$.

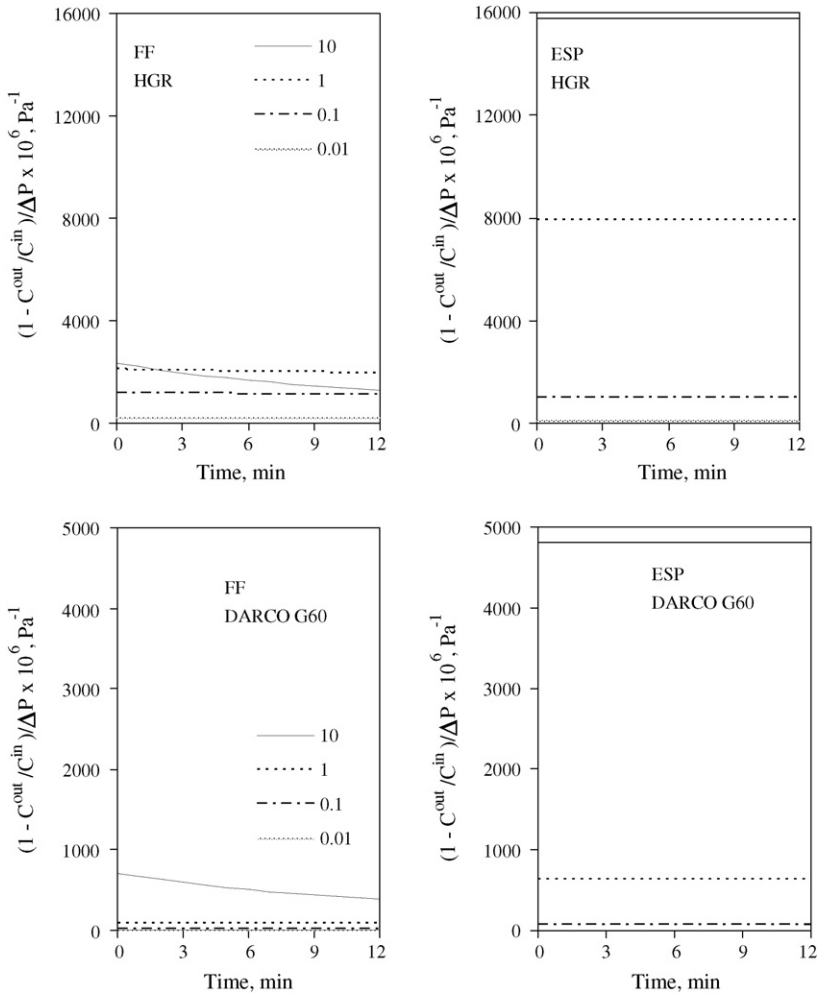

Fig. 7. Fractional mercury uptake per-unit-pressure-drop for HGR (up) in a FF (left) and ESP (right) and for DARCO G60 (down) in a FF (left) and ESP (right) as function of sorbent mass loading Θ_{AC}. $d_p = 20\ \mu m$; $c_B^{IN} = 5\ \mu g/m^3$; $E = 200\ kV/m$.

[18], while the Darcy equation (Eq. (15)) was used to calculate the pressure drop across the fabric filter as a function of time and sorbent mass loading:

$$\Delta P = S_E U + K_2 \Theta_{AC} U^2 t \quad (15)$$

The first term of Eq. (15) represents the constant drag of the fabric filter and the second term represents the time-varying drag of the accumulating dust cake. Representative values were used for S_E and K_2 [17], although both quantities vary widely and most often must be determined experimentally. A value of superficial velocity $U = 0.02$ m/s was used for the four different particle mass loading values Θ_{AC} and two different sorbents examined previously. The results in Fig. 7 indicate that for the highest sorbent mass loading of DARCO G60 ($\Theta_{AC} = 10$ g/m^3), the mercury uptake per-unit-pressure-drop in an ESP is initially a factor of seven greater than that in a fixed sorbent bed, increasing to a factor of 12 at the end of the bag cleaning cycle (12 min). For a lower sorbent mass loading ($\Theta_{AC} = 0.1$ g/m^3) the growth of the dust cake is a much smaller component of the overall pressure drop and the per-unit-pressure-drop performance of an ESP is nominally a constant 6.7 times that of a fixed sorbent bed over the entire bag cleaning cycle. Interestingly, the comparison exhibits a crossover when considering the higher capacity HGR sorbent. For the highest sorbent mass loading of HGR ($\Theta_{AC} = 10$ g/m^3), the behavior is the same as for DARCO G60, initially the ESP performance is a factor of seven greater, increasing to a factor of 12 greater at the end of the bag cleaning cycle. However, for an HGR sorbent mass loading of 0.1 g/m^3, the performance of the ESP has dropped slightly below (−10%) that of the fixed sorbent bed over the entire bag cleaning cycle. At such low sorbent mass loadings, however, the occurrence of the crossover would vary greatly as a function of the pressure drop of the fabric filter material used (the first term in Eq. (15)). These results are in contrast to the sorbent uptake per-unit-mass comparison, in which a fixed sorbent bed holds an advantage only for the case of a high-capacity sorbent.

4. Conclusions

The present analyses compare for the first time predictions of mercury capture by in-flight adsorption within an ESP and by fixed bed adsorption across the dust cake on a fabric filter. The comparisons show that for relatively low-capacity sorbents, little difference exists between fixed bed and in-flight adsorption on an absolute mercury removal efficiency basis. Although the fixed sorbent bed outperforms in-flight adsorption within an ESP on an absolute and a per-unit-sorbent-mass basis, the opposite is true when comparisons are made on a per-unit-pressure-drop basis. Thus, an optimal configuration for mercury adsorption for existing sources would have to balance the costs of higher sorbent injection rates with an ESP against the costs of sustaining the pressure drop across a retrofitted fabric filter.

References

[1] J.H. Pavlish, E.A. Sondreal, M.D. Mann, E.S. Olson, K.C. Galbreath, D.L. Laudal, S.A. Benson, Status review of mercury control options for coal-fired power plants, Fuel Proc. Technol. 82 (2003) 89–165.

[2] T.D. Brown, D.N. Smith, R.A. Hargis Jr., W.J. O'Dowd, Mercury measurement and its control: what we know, have learned, and need to further investigate, J. Air Waste Manage. Assoc. 49 (1999) 628–640.

[3] M. Rostam-Abadi, R. Chang, S. Chen, T. Lizzio, C. Richardson, S. Sjostrom, Demonstration of sorbent injection process for Illinois coal mercury, Final Technical Report, Illinois Clean Coal Institute Project Number 00-1/2.2D-1 (2001).

[4] H.L. Clack, Mass transfer within electrostatic precipitators: trace gas adsorption by sorbent-covered plate electrodes, J. Air Waste Manage. Assoc. 56 (2006) 759–766.

[5] H.L. Clack, Mass transfer within electrostatic precipitators: in-flight adsorption of mercury by charged suspended particulates, Environ. Sci. Technol. 40 (2006) 3617–3622.

[6] H.L. Clack, Particle size distribution effects on gas-particle mass transfer within electrostatic precipitators, Environ. Sci. Technol. 40 (2006) 3929–3933.

[7] F.B. Meserole, R. Chang, T.D. Carey, J. Machac, C.F. Richardson, Modeling mercury removal by sorbent injection, J. Air Waste Manage. Assoc. 49 (1999) 694–704.

[8] F. Scala, Simulation of mercury capture by activated carbon injection in incinerator flue gas. 2: Fabric filter removal, Environ. Sci. Technol. 35 (2001) 4373–4378.

[9] J.R.V. Flora, R.A. Hargis, W.J. O'Dowd, H.W. Pennline, R.D. Vidic, Modeling sorbent injection for mercury control in baghouse filters. I: Model development and sensitivity analysis, J. Air Waste Manage. Assoc. 53 (2003) 478–488.

[10] F. Scala, Modeling mercury capture in coal-fired power plant flue gas, Ind. Eng. Chem. Res. 43 (2004) 2575–2589.

[11] F. Scala, Simulation of mercury capture by activated carbon injection in incinerator flue gas. 1: In-duct removal, Environ. Sci. Technol. 35 (2001) 4367–4372.

[12] D. Karatza, A. Lancia, D. Musmarra, F. Pepe, Adsorption of metallic mercury on activated carbon, Proc. Combust. Inst. 26 (1996) 2439–2445.

[13] D. Karatza, A. Lancia, D. Musmarra, S. Russo, Capture of elemental mercury vapors by sulfur impregnated activated carbon, submitted for publication.

[14] J.R.V. Flora, R.A. Hargis, W.J. O'Dowd, A. Karash, H.W. Pennline, R.D. Vidic, The role of pressure drop and flow redistribution on modeling mercury control using sorbent injection in bughouse filters, J. Air Waste Manage. Assoc. 56 (2006) 343–349.

[15] J. Villadsen, M.L. Michelsen, Solution of Differential Equation Models by Polynomial Approximation, Prentice-Hall, Englewood Cliffs, 1978.

[16] H.J. White, Industrial Electrostatic Precipitation, Addison-Wesley, Reading, 1963.

[17] S. Calvert, H.M. Englund, Handbook of Air Pollution Technology, John Wiley & Sons, New York, 1984.

[18] W.T. Davis (Ed.), Air Pollution Engineering Manual/Air & Waste Management Association, John Wiley & Sons, New York, 2000.

[19] G.L. Leonard, M. Mitchner, S.A. Self, Particle transport in electrostatic precipitators, Atmos. Environ. 14 (1980) 1289–1299.

[20] J.M. Crowley, Fundamentals of Applied Electrostatics, Wiley, New York, 1986.

[21] S.K. Friedlander, Smoke, Dust, and Haze, Fundamentals of Aerosol Dynamics, second ed., Oxford University Press, Oxford, 2000.

[22] N. Frossling, The evaporation of falling drops, Gerlands Beitr. Geophys. 52 (1938) 170–216 (in German).